

A Z-scheme visible light-driven Ag₃PO₄/CeO₂ composite and its application for Rhodamine B degradation

Wen Zhou¹, Wenhui Liu^{2,*}, and Shuangqi Hu^{1,*}

¹ Environmental and Safety Engineering Institute, North University of China, Taiyuan, Shanxi 030051, People's Republic of China

² The Graduate School, North University of China, Taiyuan, Shanxi 030051, People's Republic of China

*E-mail: wenhuiliuzb@163.com, shuangqihuzb@163.com

Received: 24 December 2019 / Accepted: 23 February 2020 / Published: 10 April 2020

Efficient, visible-light-driven Ag₃PO₄/CeO₂ composites with various concentrations Ag₃PO₄ were synthesized using a simple two-step method. The photocatalysts were characterized by various morpho-structural and optical methods, such as XRD, SEM, TEM, HR-TEM, EDX, SAED, XPS and DRS. The photocatalytic performance of Ag₃PO₄/CeO₂ composites was investigated by the photodegradation of Rhodamine B. The results shown that the photocatalytic degradation rate of 3:1 Ag₃PO₄/CeO₂ reached 95% in 36 minutes, which is 1.6 times higher than the yield of pure Ag₃PO₄. The photocatalytic efficiency was the lowest for pure CeO₂, reaching only 9% within 36 min. Cycling runs of 3:1-Ag₃PO₄/CeO₂ to RhB 59% is higher than that of Ag₃PO₄ 32%, which demonstrates that the combination and synergistic effect of CeO₂ and Ag₃PO₄ can improve the stability of photocatalyst. After active species capture experiments, a Z-scheme reaction mechanism was also presented to elucidate the mechanism of the photocatalytic degradation process shown by the composites.

Keywords: Composite; Photocatalytic degradation; Z-scheme.

1. INTRODUCTION

Semiconductor-based photocatalysis has drew much attention due to its potential applicability to exploit the abundant solar energy to solve energy-and environmental-related issues[1-3]. Among many photocatalytic materials, CeO₂, which has a cubic structure similar to CaF₂ fluorite, has the characteristics of n-type semiconductor, possessing particular electronic orbital structure, unique optical properties, strong adsorption selectivity, excellent thermal stability and conductivity. As a photocatalyst, it also has an excellent ability to store and release oxygen[4, 5]. Compared with the traditional photocatalytic material of TiO₂, CeO₂ has a band gap of 2.92eV, which shows an increased response toward the excitation using visible light irradiation; thus, it can directly catalyze

photocatalytic degradation utilizing sunlight[6]. However, the high recombination rate of the as-generated photogenerated electron-hole pairs is still the main limiting factor for its practical applicability. Therefore, researchers have been working hard to find new strategies to improve the photocatalytic activity of the photoactive materials mentioned above. It has been found that combining the main photocatalyst with other semiconductors can effectively improve the separation and the lifetime of the photogenerated charge carriers, improving in this way the photocatalytic performance. So far, various CeO₂-based composite materials with a visible light response, such as ZnO-CeO₂[7], CeO₂/TiO₂[8], CeO₂/g-C₃N₄[9] have been reported. The heterojunction photocatalysts can expand the range of the photoresponse range and increases the absorption intensity. Due to the synergies between components, the charge carriers can be transferred in a variety of ways in order to increase the efficiency of charge separation. However low photon absorption efficiency remains a significant obstacle to the practical application of CeO₂-based composite materials. Therefore, it is an urgent task to find a suitable photosensitizer to improve the properties of the CeO₂-based composites.

Ye et al. reported results in 2010 regarding an Ag₃PO₄ based, visible light active photocatalyst, degrading organic pollutants. Since then, Ag₃PO₄ photocatalysts have been extensively investigated[10]. This photocatalyst has a body-centered cubic structure with a band gap of ≈ 2.36 eV. It exhibits an excellent photocatalytic activity toward the decomposition of organic pollutants under visible light irradiation, and its quantum efficiency reaches $\approx 90\%$, which is much higher than in the case of other metal oxides. However, Ag₃PO₄ is vulnerable to photocorrosion in the process of photocatalytic reaction, which limits its practical applicability spectra. Therefore, researchers use a variety of methods to solve this problem, such as by designing different nanostructures of Ag₃PO₄, or by combining Ag₃PO₄ with other semiconductors, such as Ag₃PO₄/TiO₂[11], AgX/Ag₃PO₄(X=Cl,Br,I)[12]. The results showed that the combination of Ag₃PO₄ with other semiconductors could improve the structural defects of its charge carrier recombination and design a more stable composite photocatalyst.

Based on the aspects mentioned, in the present research, nano-CeO₂ was prepared by hydrothermal-solvot method, and then nano-Ag₃PO₄ was deposited using in situ synthesis at room temperature to obtain the Ag₃PO₄/CeO₂ composite photocatalyst.

2. EXPERIMENTAL PART

2.1. Reagents

Cerium nitrate (Ce(NO₃)₃·6H₂O), sodium hydroxide (NaOH), silver nitrate (AgNO₃), disodium hydrogen phosphate (Na₂HPO₄·12H₂O), absolute ethanol, and rhodamine B were all analytically pure.

2.2. Preparation of catalyst

2.2.1. Preparation of CeO₂

Add 1.74g of Ce(NO₃)₃·6H₂O to 40ml of deionized water and stirred for 30min. 20ml (1 mol/L) of NaOH solution was quickly added into the above solution, stirred vigorously for one hour,

and placed in a high pressure reactor at 180°C for 18h. The mixture was separated by natural cooling, washed, and the precipitate was collected and placed in the oven at 60°C for 24 hours. The precipitate was heated in a muffle furnace at a rate of 5°C/min to 300°C and calcined for 4 h. After cooling by radiation, the yellow CeO₂ powder can be obtained.

2.2.2. Preparation of Ag₃PO₄/CeO₂ Composites

0.1g of CeO₂ powder was added to a solution of 0.612g of AgNO₃ in 30mL of silver nitrate, and sonicated for 30min to uniformly disperse CeO₂. A 30mL solution containing 0.43g of Na₂HPO₄·12H₂O was added and stirred for 120min. The sediment was centrifuged, the product was washed with ultra-pure water and absolute ethanol, and the precipitate was collected and dried. The products was named as 2:1 Ag₃PO₄/CeO₂ for its molar mass ratio is n(Ag₃PO₄):n(CeO₂)=2:1. The Ag₃PO₄/CeO₂ composite with a molar mass ratio of 3:1 and 4:1 was also prepared by increasing the amount of AgNO₃ and Na₂HPO₄·12H₂O while maintaining the quality of CeO₂, and named it 3:1 Ag₃PO₄/CeO₂ and 4:1 Ag₃PO₄/CeO₂ composites. Ag₃PO₄ was prepared under the same conditions as above except without adding CeO₂.

2.3. Characterization

LAMBDA35 Ultraviolet/visible spectrophotometer; DR-MS30 Derui Ultrasonic cleaner; WG9140B electrothermal blast drying oven; JOYN-GHX-DC photochemical reactor; JSM-6510 scanning electron microscope; Rigaku D/max-2500 X-ray diffractometer; JEM-2100 high-resolution transmission electron microscope; ESCALAB 250 X-ray photoelectron spectrometer; UV-2550 UV-visible diffuse reflectance absorption spectrometer.

2.4. Photocatalysis experiment

Photocatalysis experiments were completed in a JOYN-GHX-DC photochemical reactor. Using a 1000W xenon lamp as the visible light source, weigh 50mg of the prepared photocatalyst, disperse it into a test tube containing 50mL of 10mg/L RhB, put it into the photochemical reactor, and close the door to avoid the light and stir for 20min to make the catalyst can be evenly dispersed. Then turn on the light source and sample 4mL every 6 min. The sample taken is centrifuged and the supernatant is taken. The absorbance of the RhB solution before and after the reaction was measured at 550nm using an ultraviolet-visible spectrophotometer. During the reaction, the temperature of the reaction suspension was controlled at about 10 °C by circulating water. The decolorization rate of RhB by photocatalytic degradation was calculated by using Bill Lambert's law (1); The photocatalytic degradation of RhB was characterized by kinetic equation (2); Thus to judge the photocatalytic degradation performance of the photocatalyst.

$$C_t/C_0 = A_t/A_0 \quad (1)$$

$$A_t + Kt = -\ln (C_t/C_0) \quad (2)$$

Where A_0 and A_t represent the absorbance of the solution after the initial and illumination t time, respectively, and C_0 and C_t mean the corresponding original concentration of the solution and the instantaneous concentration of the solution after t time.

Catalyst cycle stability analysis: The photocatalyst after each use was collected, and after repeated washing and drying, the above procedure was repeated 3 times to examine the cycle stability.

3. RESULT AND DISCUSSION

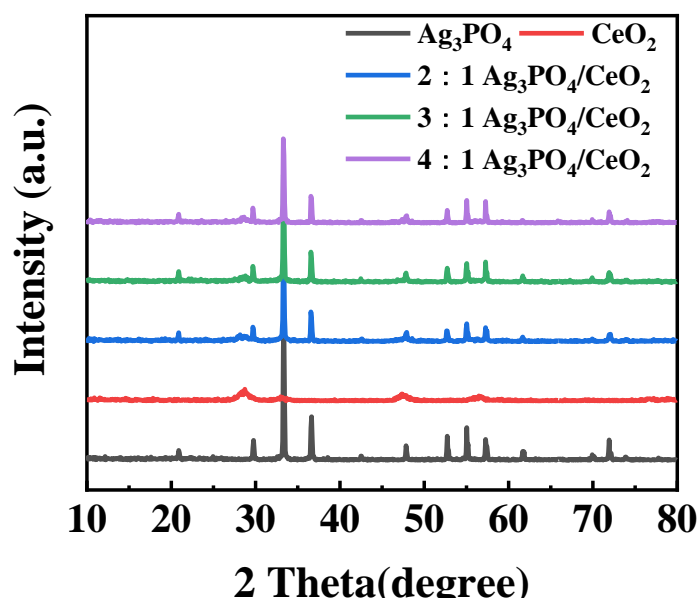


Figure 1. The XRD patterns of the as-prepared samples

The crystal structure phase of the catalyst were examined by XRD analysis. Fig. 1 is an XRD spectrum of the prepared $\text{Ag}_3\text{PO}_4/\text{CeO}_2$, 2:1 $\text{Ag}_3\text{PO}_4/\text{CeO}_2$, 3:1 $\text{Ag}_3\text{PO}_4/\text{CeO}_2$, 4:1 $\text{Ag}_3\text{PO}_4/\text{CeO}_2$ catalyst. From the Ag_3PO_4 XRD spectrum, the inflection peaks at 20.9° , 29.7° , 33.3° , 36.6° , 47.9° , 52.7° , 55.1° , 57.4° , 61.7° , 72.0° belong to Ag_3PO_4 (JCPDS No. 70-0702) trait peaks of (110), (200), (210), (211), (310), (222), (320), (321), (400), (421) crystal planes[11]. For the monomeric CeO_2 , main diffraction peaks were observed at 28.5° , 33.1° , 47.5° , and 56.3° , and these diffraction peaks were matched with the crystal faces (111), (200), (220), and (311) of CeO_2 (JCPDS No. 78-0694). The composite photocatalyst produced exhibited characteristic peaks consistent with CeO_2 and Ag_3PO_4 , which indicates that the $\text{Ag}_3\text{PO}_4/\text{CeO}_2$ composite has been successfully synthesized. In addition, with the increase of the Ag_3PO_4 content in the composite, the peak intensity of the feature peak (111) of CeO_2 on the composite gradually weakens.

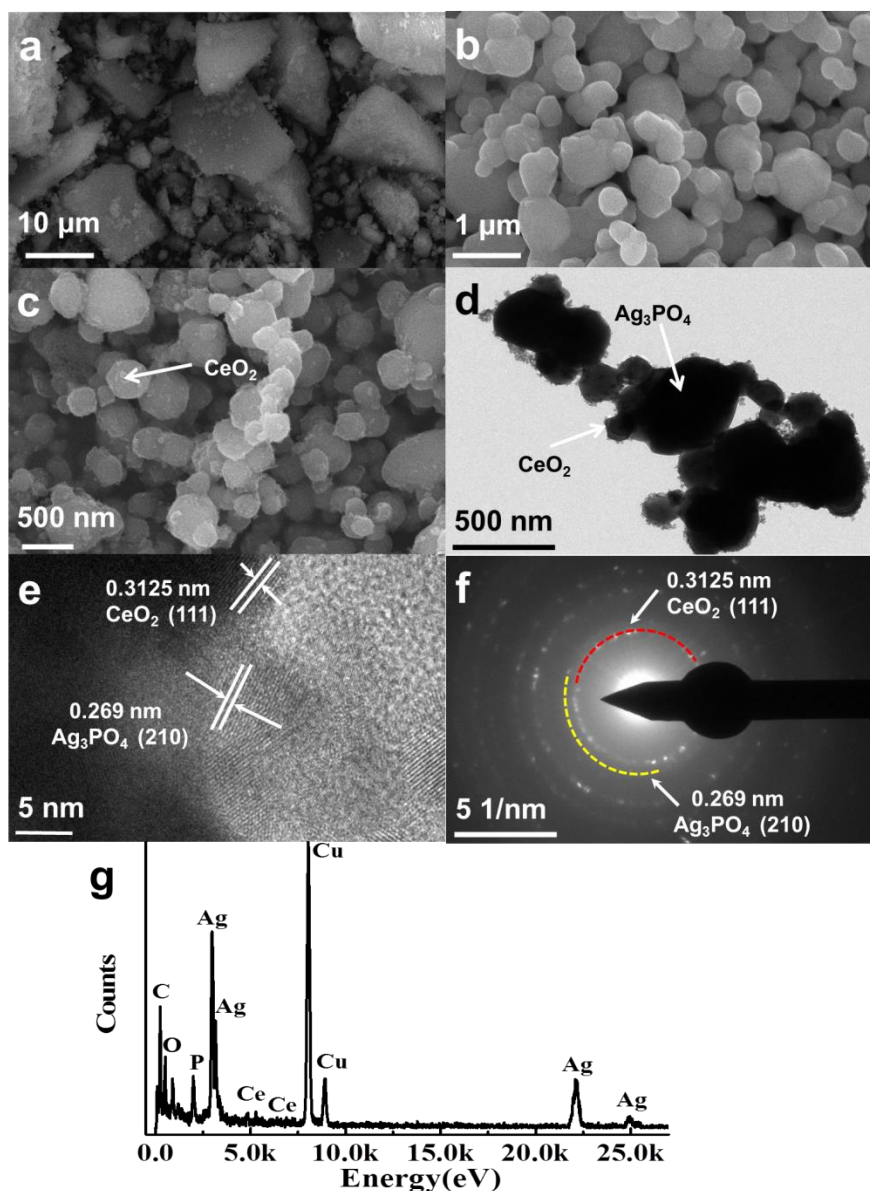


Figure 2. SEM images of prepared photocatalysts: a CeO_2 , b Ag_3PO_4 , c $\text{Ag}_3\text{PO}_4/\text{CeO}_2$, d TEM image of $\text{Ag}_3\text{PO}_4/\text{CeO}_2$, e HRTEM image of $\text{Ag}_3\text{PO}_4/\text{CeO}_2$, SAED image of $\text{Ag}_3\text{PO}_4/\text{CeO}_2$ and g corresponding EDX pattern of $\text{Ag}_3\text{PO}_4/\text{CeO}_2$

Fig. 2 is the SEM, TEM, SAED, and EDX diagram of CeO_2 , Ag_3PO_4 , $\text{Ag}_3\text{PO}_4/\text{CeO}_2$ catalysts. Fig. 2a is the bulk nano- CeO_2 prepared by solvothermal method. Regular hexahedral structure Ag_3PO_4 crystal with particle size ranging from 0.5 to 1 μm can be observed in Fig. 2b. SEM image of $\text{Ag}_3\text{PO}_4/\text{CeO}_2$ after composite has been displayed in Fig. 2c and the surface of Ag_3PO_4 enriches the CeO_2 nanoparticles. Fig. 2d is the TEM image of $\text{Ag}_3\text{PO}_4/\text{CeO}_2$ and the nano- CeO_2 particles about 100 nm are attached to the Ag_3PO_4 surface, this preparation method of wrapped $\text{Ag}_3\text{PO}_4/\text{CeO}_2$ can also be demonstrated by Lin[13]. The HRTEM of $\text{Ag}_3\text{PO}_4/\text{CeO}_2$ is shown in Fig. 2e. The tight bonding of CeO_2 particles to Ag_3PO_4 , and the lattice spacing d are 0.3125 and 0.269 nm, representing the (111) crystal plane of CeO_2 and (210) crystal plane of Ag_3PO_4 , respectively. Fig. 2f is the SAED of $\text{Ag}_3\text{PO}_4/\text{CeO}_2$ and the bright diffraction ring of $\text{Ag}_3\text{PO}_4/\text{CeO}_2$ indicates that it is polycrystalline. In

addition, the lattice spacing of the two crystal faces in Fig. 2f is 0.3125 nm and 0.269 nm, respectively, which is in good agreement with the results of high resolution transmission electron microscopy. Fig. 2g is the EDX diagram of $\text{Ag}_3\text{PO}_4/\text{CeO}_2$ and four elements: Ce, O, Ag, and P can be found, which is corresponding to the chemical elements of $\text{Ag}_3\text{PO}_4/\text{CeO}_2$ [14]. The apparent Cu element diffraction peak is generated by the Cu mesh used to prepare the test sample during TEM test. Through the above analysis and discussion, it can be clearly determined that CeO_2 is dispersed in the form of particles to the surface of Ag_3PO_4 crystal and has a good hexahedral morphology.

To study the surface chemical state of $\text{Ag}_3\text{PO}_4/\text{CeO}_2$, we used XPS technology to analyze its surface chemical state at Fig. 3. The photoelectron spectroscopy full-spectrum scan of $\text{Ag}_3\text{PO}_4/\text{CeO}_2$ composites is indicated in Fig. 3a. Fig. 3b is the XPS spectrum of the sample Ce 3d, and the Ce 3d XPS spectrum of CeO_2 is composed of two multi-state peaks corresponding to Ce $3d_{5/2}$ and Ce $3d_{3/2}$, respectively[15,16]. Fig. 3c is the emission spectrum of Ag 3d. The peaks appear at 376.5 eV and 382.4 eV, matching with Ag $3d_{5/2}$ and Ag $3d_{3/2}$, respectively.

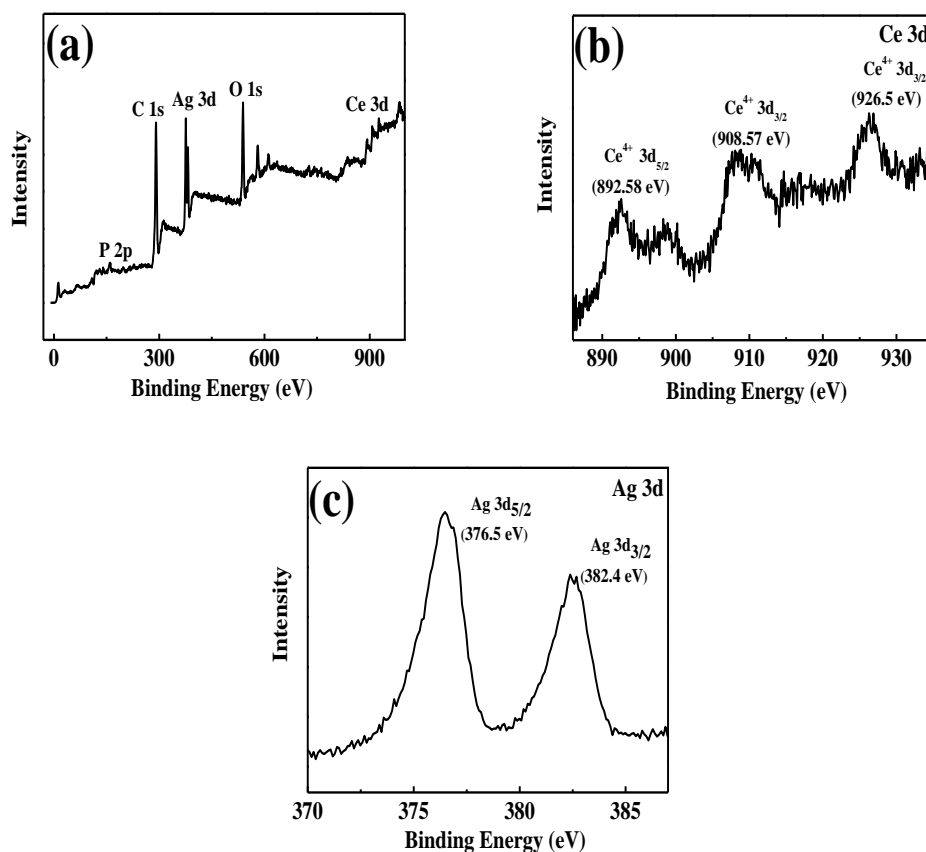


Figure 3. XPS spectrum of $\text{Ag}_3\text{PO}_4/\text{CeO}_2$: (a) survey scan, (b) Ce 3d, (c) Ag 3d

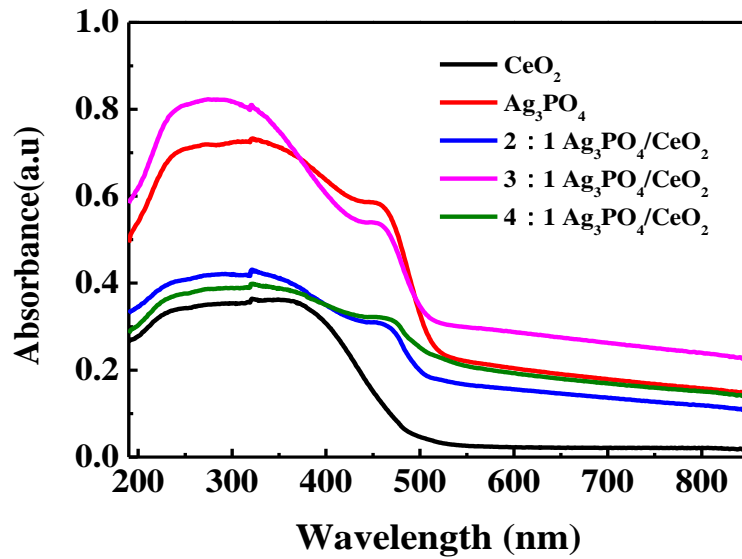


Figure 4. UV-Vis DRS of CeO_2 , Ag_3PO_4 , $2:1\text{Ag}_3\text{PO}_4/\text{CeO}_2$, $3:1\text{Ag}_3\text{PO}_4/\text{CeO}_2$, $4:1\text{Ag}_3\text{PO}_4/\text{CeO}_2$ catalysts

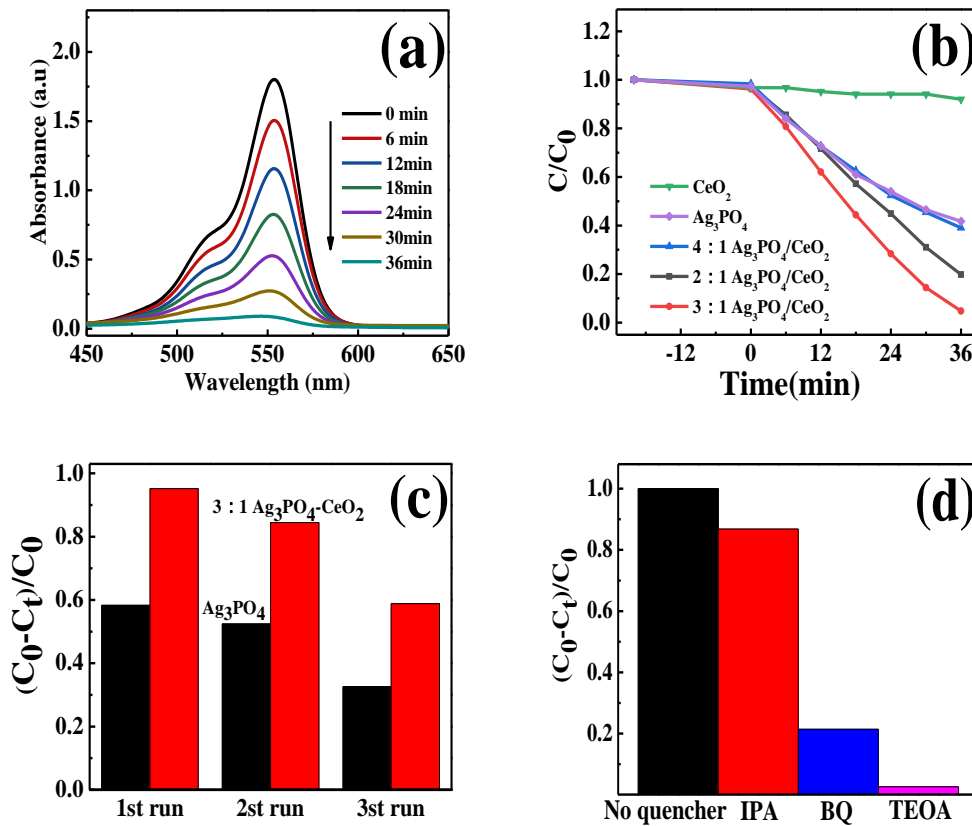


Figure 5. (a) Visible light scanning patterns of $\text{Ag}_3\text{PO}_4/\text{CeO}_2$ degradation of RhB; (b) Effects of different catalysts on photocatalytic degradation of RhB under visible light; (c) Cycling runs of Ag_3PO_4 and $\text{Ag}_3\text{PO}_4/\text{CeO}_2$ for the degradation of RhB; (d) Trapping experiments of active species

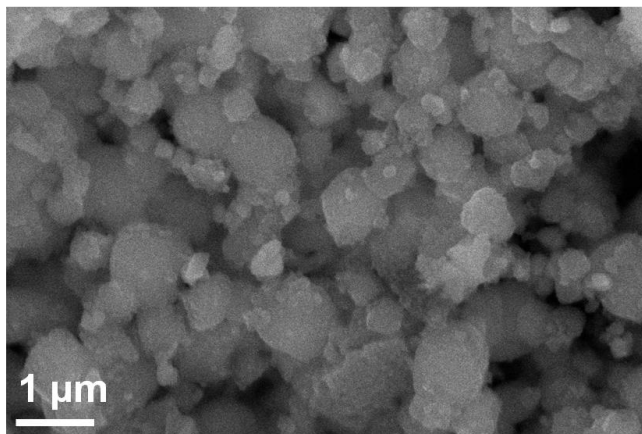


Figure 6. The SEM image of 3:1Ag₃PO₄/CeO₂ after 3 cycles of use

Fig. 4 shows the UV-visible diffuse reflectance spectra of CeO₂, Ag₃PO₄, 2:1Ag₃PO₄/CeO₂, 3:1Ag₃PO₄/CeO₂, 4:1Ag₃PO₄/CeO₂ catalysts. From the Fig. 4, the cutoff wavelengths of CeO₂ and Ag₃PO₄ are at 475 nm and 500 nm, which are in agreement previous reports[13,17]. After supporting CeO₂ onto the Ag₃PO₄, the optical absorption wavelength is broadened, and the absorption intensity is enhanced. The optical absorption effect of 3:1Ag₃PO₄/CeO₂ is the best, indicating that the interaction between Ag₃PO₄ and CeO₂ in the Ag₃PO₄/CeO₂ composite system can strengthen the photocatalytic properties of the composite.

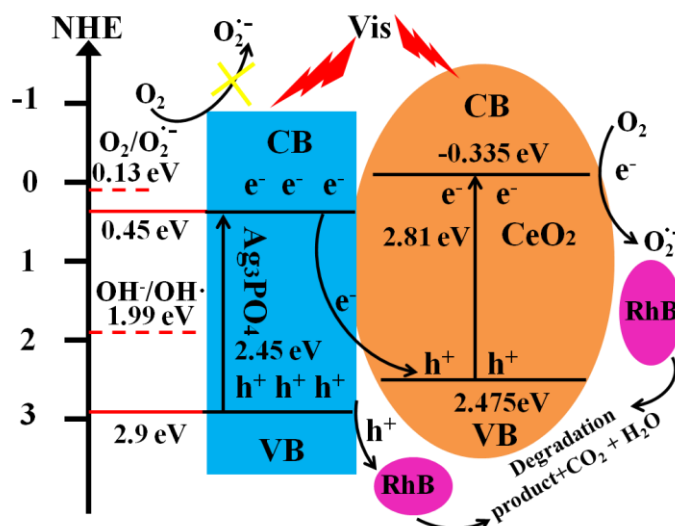
The changes of RhB molecule during photocatalytic degradation of 3:1Ag₃PO₄/CeO₂ was analyzed by UV-visible full-wavelength scanning in Fig. 5a. The RhB characteristic peak at 553 nm gradually weakened with the reaction progress. The peak disappears after 36 min of illumination, suggesting that the azo structure of RhB dye was wiped out.

Fig. 5b shows the degradation effect of different catalysts CeO₂, Ag₃PO₄, 2:1Ag₃PO₄/CeO₂, 3:1Ag₃PO₄/CeO₂, 4:1Ag₃PO₄/CeO₂ on RhB. The results show that the pure CeO₂ photocatalytic degradation rate is the worst only 9% within 36 min. The photocatalytic degradation rates of Ag₃PO₄, 2:1Ag₃PO₄/CeO₂, 4:1Ag₃PO₄/CeO₂ at 36 min were 59%, 80%, and 61%, respectively. The catalytic effect of 3:1 Ag₃PO₄/CeO₂ catalyst is the best. The photocatalytic degradation rate reaches 95% in 36min, which is 1.6 times that of pure Ag₃PO₄. The results illustrate that CeO₂ can obviously improve the photocatalytic degradation performance of Ag₃PO₄ photocatalyst.

Fig. 5c shows the stability test results of Ag₃PO₄ and 3:1Ag₃PO₄/CeO₂ recycled three times. It can be seen from the figure that after three times of recycling, the degradation rate of Ag₃PO₄ to RhB is only 32%, while the degradation rate of 3:1Ag₃PO₄/CeO₂ to RhB is 59%, which shows that the combination of CeO₂ and Ag₃PO₄ can improve the stability of photocatalyst. It has also been proved by other literatures that the high photocatalytic stability can be obtained by compounding[18]. Fig. 6 is the SEM image of 3:1Ag₃PO₄/CeO₂ after 3 cycles of use. It can be found that the catalyst morphology is basically stable, indicating that the material structure is relatively stable. Therefore, it has good photocatalytic degradation performance after three times of recycles.

Fig. 5d displays the results of different capture agents on the photocatalytic degradation rate of RhB by 3:1 Ag₃PO₄/CeO₂. The addition of IPA has little effect on the degradation of RhB, indicating

that almost no hydroxyl radical ($\text{OH}\cdot$) is produced during the degradation process. While the addition of BQ and TEOA to the reaction system, the photocatalytic process was evidently inhibited. So, we can speculate that the oxidation process of hole (h^+) and superoxide anion (O_2^-) are the main active species in the 3:1 $\text{Ag}_3\text{PO}_4/\text{CeO}_2$ photocatalytic degradation process on RhB.



Scheme 1.the photocatalytic mechanism illustration of $\text{Ag}_3\text{PO}_4/\text{CeO}_2$

Based on the above photocatalytic and free radical trap experiments, a possible Z-scheme reaction mechanism was proposed. The valence band and conduction band width levels of Ag_3PO_4 are ca. 0.45 eV and 2.9 eV (vs. NHE), the forbidden band width is 2.45 eV [10,19]. The valence band and conduction band levels of CeO_2 are ca. -0.335 eV and 2.475 eV (vs. NHE), the forbidden band width of CeO_2 is 2.81 eV [20]. Both Ag_3PO_4 and CeO_2 can undergo electronic transitions to generate photogenerated electron-hole pairs with visible light irradiation. The energy of photogenerated holes formed by Ag_3PO_4 is about 2.9 eV, which is greater than $E(\text{OH}^-/\text{OH}\cdot)$ the reaction potential of $\text{OH}^-/\text{OH}\cdot$. Thus, the holes generated on the Ag_3PO_4 valence band can be combined with the OH^- formed by ionization of H_2O to form $\text{OH}\cdot$, which further participates in the degradation of organic pollutants [21]. Since the photogenerated electron energy formed by Ag_3PO_4 is smaller than $E(\text{O}_2/\text{O}_2^-)$ the activation energy of single electron oxygen, the photogenerated electrons on the Ag_3PO_4 conduction band cannot combine with the dissolved oxygen in the solution. The photogenerated electron energy generated by CeO_2 is larger than $E(\text{O}_2/\text{O}_2^-)$, and the activity electrons generated on the CeO_2 conduction band can be united in the dissolved oxygen to generate superoxide anion (O_2^-), which further participates in the degradation reaction. The photogenerated holes formed on valence band cannot form $\text{OH}\cdot$ due to the reaction potential energy lower than $E(\text{OH}^-/\text{OH}\cdot)$. As the backlog of photogenerated electrons on the Ag_3PO_4 conduction band, it can recombine with the photogenerated holes accumulated in the CeO_2 valence band, thus its photocatalytic performance can be improved by enhancing the separation efficiency of $\text{Ag}_3\text{PO}_4/\text{CeO}_2$ composite photogenerated electron-hole pairs.

4. CONCLUSION

The photoactive visible-light-driven $\text{Ag}_3\text{PO}_4/\text{CeO}_2$ composites with different Ag_3PO_4 contents were prepared by a two-step method. The optical absorption range and intensity in the wavelengths of the 3:1- $\text{Ag}_3\text{PO}_4/\text{CeO}_2$ were proved to be higher than that of pure CeO_2 and Ag_3PO_4 , as the photocatalytic degradation rate of 3:1- $\text{Ag}_3\text{PO}_4/\text{CeO}_2$ reached 95% in 36min, which was 1.6 times higher than that of pure Ag_3PO_4 . After three times of recycling, the degradation rate of 3:1- $\text{Ag}_3\text{PO}_4/\text{CeO}_2$ to RhB was 59%, being higher than that of Ag_3PO_4 32%, which demonstrates that the combination of CeO_2 and Ag_3PO_4 can improve the stability of photocatalyst. A Z-scheme reaction mechanism was also proposed to elucidate the photocatalytic degradation process of the $\text{Ag}_3\text{PO}_4/\text{CeO}_2$ composites.

References

1. A. Fujishima, K. Honda *Nature*, 238(1972) 37.
2. K. Shen, M.A. Gondal, R.G. Siddique, S. Shi, Q. *Chinese Journal of Catalysis*, 35 (2014) 78.
3. Y. Wang, L. Liu, D. Wu, J. Guo, J. Shi, J. Liu, C. Su, *Chinese Journal of Catalysis*, 40 (2019) 1198.
4. A.D. Liyanage, S.D. Perera, K. Tan, Y. Chabal, J.K.J. Balkus, *ACS Catalysis.*, 4 (2014) 577-584.
5. W. Lei, T. Zhang, L. Gu, P. Liu, J.A. Rodriguez, G. Liu, M. Liu, *ACS Catalysis.*, 5 (2015) 4385.
6. F. Chen, Y. Cao, D. *Applied Surface Science*, 257 (2011) 9226.
7. C. Li, C. Rui, X. Zhang, S. Shu, X. Jie, Y. Zheng, W. Dong, *Materials Letters*, 65 (2011) 1327.
8. X. Lu, X. Li, J. Qian, N. Miao, Y. Chao, Z. Chen, *Journal of Alloys & Compounds*, 661 (2016) 363.
9. X. She, H. Xu, H. Wang, J. Xia, Y. Song, J. Yan, Y. Xu, *Dalton Trans.*, 44 (2015) 7021.
10. Z. Yi, J. Ye, N. Kikugawa, T. Kako, S. Ouyang, H. Stuart-Williams, H. Yang, J. Cao, W. Luo, Z. Li, *Nature Materials*, 9 (2010) 559.
11. W. Liu, D. Liu, K. Wang, X. Yang, L. Hu, *Nanoscale Research Letters*, 14 (2019) 203-211.
12. W. Wang, H. Du, R. Wang, T. Wen, A. Xu, *Nanoscale*, 5 (2013) 3315.
13. W. Lin, S. Zhang, D. Wang, C. Zhang, D. Sun, *Ceramics International*, 41(2015) 8956.
14. Y. Song, H. Zhao, Z. Chen, W. Wang, L. Huang, H. Xu, H. Li, *Phys. Status Solidi (A)*, 9(2016)213.
15. H. Kim, M.A.I. Shuvo, H. Karim, M.I. Nandasiri, Y. Lin, *MRS Advances*, 2 (2017) 1.
16. M. Khan, W. Khan, M. Ahamed, A.N. Alhazaa, *Scientific Reports*, 7 (2017) 12560.
17. X. Wen, C. Niu, M. Ruan, *Journal of Colloid and Interface Science*, 497 (2017) 368.
18. Z. Yang, G. Huang, W. Huang, *Journal of Materials Chemistry. A*, 2 (2014) 1750.
19. Y. An, P. Zheng, X. Ma, *RSC Advances*, 9 (2019) 721.
20. X.J. Wen, C.-G. Niu, M. Ruan, L. Zhang, G.-M. Zeng, *Journal of Colloid & Interface Science*, 497 (2017) 368.
21. S. Dong, L. Hu, J. Feng, Y. Pi, Q. Li, Y. Li, M. Liu, J. Sun, J. Sun, *Rsc Advances*, 4 (2014) 64994